BIOMOLECULES & THERAPEUTICS

Original Article
Biomol Ther 28(2), 195-201 (2020)

Functional Expression of Choline Transporter-Like Protein 1 in LNCaP Prostate Cancer Cells: A Novel Molecular Target

Iwao Saiki[1], Miki Yara[1], Tsuyoshi Yamanaka[2], Hiroyuki Uchino[1] and Masato Inazu[2,3,*]

[1]Department of Anesthesiology, Tokyo Medical University, Tokyo 160-0023,
[2]Department of Molecular Preventive Medicine, Tokyo Medical University, Tokyo 160-8402,
[3]Institute of Medical Science, Tokyo Medical University, Tokyo 160-8402, Japan

Abstract

Prostate cancer is one of the most common cancers in men. Choline PET or PET/CT has been used to visualize prostate cancer, and high levels of choline accumulation have been observed in tumors. However, the uptake system for choline and the functional expression of choline transporters in prostate cancer are not completely understood. In this study, the molecular and functional aspects of choline uptake were investigated in the LNCaP prostate cancer cell line along with the correlations between choline uptake and cell viability in drug-treated cells. Choline transporter-like protein 1 (CTL1) and CTL2 mRNA were highly expressed in LNCaP cells. CTL1 and CTL2 were located in the plasma membrane and mitochondria, respectively. [^{3}H]Choline uptake was mediated by a single Na^+-independent, intermediate-affinity transport system in the LNCaP cells. The anticancer drugs, flutamide and bicalutamide, inhibited cell viability and [^{3}H]choline uptake in a concentration-dependent manner. The correlations between the effects of these drugs on cell viability and [^{3}H]choline uptake were significant. Caspase-3/7 activity was significantly increased by both flutamide and bicalutamide. Furthermore, these drugs decreased CTL1 expression in the prostate cancer cell line. These results suggest that CTL1 is functionally expressed in prostate cancer cells and are also involved in abnormal proliferation. Identification of this CTL1-mediated choline transport system in prostate cancer cells provides a potential new therapeutic target for the treatment of this disease.

Key Words: Choline, Transporter, Prostate cancer, Apoptotic cell death, Caspase

INTRODUCTION

Choline is a water-soluble organic cation that is crucial for the normal function of all cells. Its cellular absorption occurs via choline transporters. After uptake, choline is metabolized and used for various functions (e.g., regulation of osmotic pressure, a precursor for methyl donors in epigenetics, phospholipid synthesis) (Michel and Bakovic, 2012; Inazu, 2014). Choline is an essential component of the membrane phospholipids phosphatidylcholine (PC) and sphingomyelin and plays a critical role in the structure and function of biological membranes in all cells. Thus, large amounts of choline uptake and PC biosynthesis are needed for new membrane synthesis. Choline is also a precursor for the synthesis of the neurotransmitter acetylcholine at the cholinergic nerve terminal. Finally, choline is converted to betaine through oxidative metabolism, which provides a source of methyl groups for the production of S-adenosylmethionine (SAM). SAM participates in DNA and histone methylation and is therefore required for the establishment and maintenance of the epigenome (Anderson *et al*., 2012).

^{11}C- or ^{18}F-labelled choline derivatives are used as diagnostic tools for positron emission tomography (PET) and PET/computed tomography (PET/CT) in clinical oncology (Schwarzenböck *et al*., 2012; Xu *et al*., 2019). Choline PET is highly effective for imaging several tumor types, including prostate carcinoma (Kotzerke *et al*., 2000), brain tumors (Ohtani *et al*., 2001), lung metastasis of esophageal cancer (Kobori *et al*., 1999), and mediastinal lymph node metastases (Hara *et al*., 2000). Choline PET can also be used to differentiate between malignant and benign lesions in various regions of the body, including the brain, head, bone, and soft tissue (Tian *et al*., 2004). Choline PET or PET/CT is increasingly used to visualize primary and recurrent prostate cancer (Hara *et al*., 1998;

Open Access **https://doi.org/10.4062/biomolther.2019.097**

Received Jun 12, 2019 **Revised** Sep 12, 2019 **Accepted** Oct 1, 2019
Published Online Nov 6, 2019

***Corresponding Author**
E-mail: inazu@tokyo-med.ac.jp
Tel: +81-3-3351-6141, Fax: +81-3-3351-6166

Xu *et al*., 2019). Because tumor cells grow very quickly, the biosynthesis of their cell membranes is also rapid. Consequently, the uptake of choline by tumors is linked to the rate of tumor cell proliferation. Intracellular uptake of choline via the choline transporter is the rate-limiting step in the synthesis of phospholipids in the plasma membrane, and a prerequisite for cancer cell proliferation. However, the uptake system for choline and the functional expression of choline transporters in human prostate cancer are not completely understood.

To date, the choline transport system has been categorized into three major transporter families: (I) high-affinity choline transporter 1 (CHT1/SLC5A7), (II) choline transporter-like proteins (CTL1-5/SLC44A1-5), and (III) polyspecific organic cation transporters (OCT1-2/SLC22A1-2) with low affinity for choline (Michel *et al*., 2006). The families are expressed in different organisms and cell types and are involved in a variety of physiological functions. Our studies have shown that many cancer cells express high levels of CTL1, and inhibition of CTL1 function induces apoptotic cell death (Inazu, 2014; Taguchi *et al*., 2014; Nishiyama *et al*., 2016; Nagashima *et al*., 2018). Thus, CTL1 may be a target for cancer therapy.

In this study, we investigated which transporters could mediate choline uptake in LNCaP prostate cancer cells, which are androgen-dependent. We also examined the correlations between choline uptake and the effects of anticancer drugs on cell viability.

MATERIALS AND METHODS

Cell culture

The human prostate adenocarcinoma cell line, LNCaP (RCB2144), PC-3 (RCB2145) and DU-145 (RCB2143) were provided by the RIKEN BRC through the National Bio-Resource Project of the MEXT (Ibaraki, Japan). The cells were grown in RPMI 1640 medium (Wako, Osaka, Japan) supplemented with 10% fetal bovine serum (Gibco BRL, Gaithersburg, MD, USA) and 20 mg/L kanamycin (Gibco BRL) in non-coated flasks. Cultures were maintained in a humidified atmosphere of 5% CO_2 and 95% air at 37°C, and the medium was changed every 3 to 4 days.

RNA extraction and real-time polymerase chain reaction (PCR)

Total RNA was extracted from cells using ISOGEN (Wako) according to the manufacturer's instructions. The primer pairs and TaqMan probes for the target (CHT1, OCT1-3, CTL1-5) and housekeeping (glyceraldehyde-3-phosphate dehydrogenase [GAPDH]) mRNAs were designed based on human mRNA sequences using TaqMan® Gene Expression Assays (Applied Biosystems, Foster City, CA, USA) (Table 1). One-step real-time PCR was performed on total RNA (50 ng) using the TaqMan® RNA-to-CT™ 1-Step Kit (Applied Biosystems) according to the manufacturer's instructions. Real-time PCR data were analyzed using the LightCycler® 96 system (Roche Diagnostics, Mannheim, Germany). Target gene expression levels were calculated relative to GAPDH using the comparative cycle time (C_t) method (relative mRNA expression=$2^{-(Ct\ target-Ct\ GAPDH)}$×100%).

Immunocytochemistry

LNCaP cells were grown in 35 mm glass base dishes (IWAKI, Chiba, Japan), washed twice with D-PBS, and fixed with 100% MeOH for 20 min at room temperature. Fixed cells were incubated with detector blocking solution (Kirkegaard and Perry Laboratories, Gaithersburg, MD, USA) overnight at 4°C. Cells were incubated with 2 μg/mL anti-CTL1 rabbit polyclonal antibody (ab110767, Abcam plc, Cambridge, UK), 2 μg/mL anti-CTL2 mouse monoclonal antibody (clone 2D11, Abnova, Taipei City, Taiwan), or anti-COX IV rabbit polyclonal antibody (ab16056, Abcam plc) in fresh blocking solution overnight at 4°C. After washing with wash solution (Kirkegaard and Perry Laboratories), the cells were incubated with 1 μg/mL Alexa Fluor 488 goat anti-mouse IgG (Molecular Probes, Eugene, OR, USA) or Alexa Fluor 568 goat anti-rabbit IgG (Molecular Probes) for 1 h at room temperature. After washing, the specimens were mounted using VECTASHIELD mounting medium containing DAPI (Vector Laboratories, Burlingame, CA, USA). Fluorescence images were obtained using a Confocal Laser Scanning Biological Microscope (FV10i-DOC, Olympus, Tokyo, Japan).

Immunoblotting

Cells were washed twice with D-PBS (Wako) and extracted on ice in RIPA buffer (Santa Cruz, CA, USA) containing 1 mM EDTA and protease inhibitors. The extracts were centrifuged for 15 min at 4°C. The supernatant was incubated for 5 min at 100°C in a 1:1 (v:v) ratio with Tris–SDS β-ME sample solution (Cosmo Bio, Tokyo, Japan). The samples electrophoresed on 10% SDS-PAGE gels and then transferred to PVDF membranes. Following protein transfer, the membranes were blocked with Detector Block Solution (Kirkegaard and Perry Laboratories) overnight at 4°C. Membranes were then in-

Table 1. TaqMan® gene expression assay

Gene	Accession number	Assay ID	Exon boundary	Assay location	Amplicon length
CHT1 (SLC5A7)	NM_021815	Hs00222367_m1	4-5	749	66
CTL1 (SLC44A1)	NM_080546	Hs00223114_m1	5-6	759	66
CTL2 (SLC44A2)	NM_020428	Hs01105936_m1	20-21	2060	67
CTL3 (SLC44A3)	NM_001114106	Hs00537043_m1	5-6	625	64
CTL4 (SLC44A4)	NM_001178044	Hs00228901_m1	12-13	1177	58
CTL5 (SLC44A5)	NM_152697	Hs01120485_m1	9-10	673	73
OCT1 (SLC22A1)	NM_003057	Hs00427554_m1	8-9	1493	66
OCT2 (SLC22A2)	NM_003058	Hs01010723_m1	10-11	1771	120
OCT3 (SLC22A3)	NM_021977	Hs01009568_m1	10-11	1657	73
GAPDH	NM_002046	Hs99999905_m1	3-3	243	122

cubated with 1 μg/mL rabbit anti-CTL1 polyclonal antibody (ab110767, Abcam plc) in new Detector Block Solution overnight at 4°C. Membranes were washed three times in wash solution and then incubated with 1 μg/mL horseradish peroxidase-conjugated anti-rabbit and anti-goat IgG (Kirkegaard and Perry Laboratories) for 1 h at room temperature. Following washing, protein bands were visualized using the ECL Prime Western Blotting Detection System (GE Healthcare Life Sciences, Marlborough, MA, USA) on the ChemiDoc XRS Plus System (Bio-Rad Laboratories, Hercules, CA, USA).

[^{3}H]Choline uptake into LNCaP cells

[^{3}H]Choline uptake was measured as previously described (Nagashima *et al*., 2018). Following removal of the growth medium, the cells were washed twice with uptake buffer (125 mM NaCl, 4.8 mM KCl, 1.2 mM $CaCl_2$, 1.2 mM KH_2PO_4, 5.6 mM glucose, 1.2 mM $MgSO_4$, and 25 mM HEPES adjusted to pH7.4 with Tris) and then incubated with [^{3}H]choline (PerkinElmer, Boston, MA, USA). When Na^+-free buffer was used, NaCl was replaced with an equimolar concentration of N-methyl-D-glucamine chloride (NMDG-Cl). Choline uptake was terminated by removal of the uptake buffer and three rapid washes with ice-cold uptake buffer. The cultures were dissolved in 0.1 M NaOH containing 0.1% Triton X-100. The radioactivity was measured using a liquid scintillation counter (Tri-Carb®2100 TR, Packard, Palo Alto, CA, USA).

Uptake buffers of varying pH (pH 6.0, 6.5, 7.0, 7.5, 8.0, and 8.5) were prepared by mixing 25 mM MES (pH 5.5) and 25 mM Tris (pH 8.5). Both buffers contained 125 mM NaCl, 4.8 mM KCl, 1.2 mM $CaCl_2$, 1.2 mMKH_2PO_4, 5.6 mM glucose, and 1.2 mM $MgSO_4$. In saturation kinetics experiments, the concentration of [^{3}H]choline was kept constant at 10 nM, and unlabeled choline was added to give the desired choline concentration. The specific uptake of [^{3}H]choline was calculated as the difference between total [^{3}H]choline uptake in the presence and absence of 30 mM unlabeled choline. Protein concentrations were determined using the DC Protein Assay Kit (Bio-Rad Laboratories).

Cell viability assay

Cells were plated, and then inhibitors were added 24 h later. Cell numbers were measured using ATPLite™ (PerkinElmer) and the luminescence ATP detection assay system according to the manufacturer's instructions. Luminescence was measured on a FilterMax F5 Multi-Mode Microplate Reader (Molecular Devices, San Jose, CA, USA).

Caspase-3/7 assay

LNCaP cells were seeded at a density of 1×10^4 cells/well in 24-well plates. Twenty-four hours after plating, cells were incubated with test drugs for 24 h. Caspase-3/7 activity was determined using the Caspase-Glo® 3/7 Assay kit (Promega Corporation, Madison, WI, USA) according to the manufacturer's instructions. Luminescence was measured on a FilterMax F5 Multi-Mode Microplate Reader (Molecular Devices).

Data analysis

Analysis of variance (ANOVA) followed by the Dunnett's multiple comparison test for data from multiple groups was performed using InStat 3 (GraphPad Software, San Diego, CA, USA). The time courses of choline uptake were compared by fitting into single-exponential decay equations. The kinetic parameters were calculated by non-linear regression methods. Eadie-Hofstee plots were fitted using linear regression (Prism 6, GraphPad Software). The K_i values were derived from the IC_{50} values as described by Cheng and Prusoff (1973): $K_i=IC_{50}/(1+[L]/K_m)$, where [L] is the concentration of radiolabeled ligand.

RESULTS

Expression of choline transporters in LNCaP, PC-3 and DU-145 cells

The expression of CHT1, CTL1-5, and OCT1-3 in prostate cancer cell lines (LNCaP, PC-3, and DU-145) was investigated using real-time PCR (Fig. 1A). In the prostate cancer cell lines, CTL1, CTL2, and CTL4 were highly expressed, and their levels did not differ from each other. In contrast, CTL3 and OCT1 were expressed at very low levels, and CHT1, CTL5, OCT2, and OCT3 were not detectable. The expression patterns of the transporters closely resembled it in all prostate cancer cell lines. Therefore, we conducted a molecular and functional analysis using LNCaP cells.

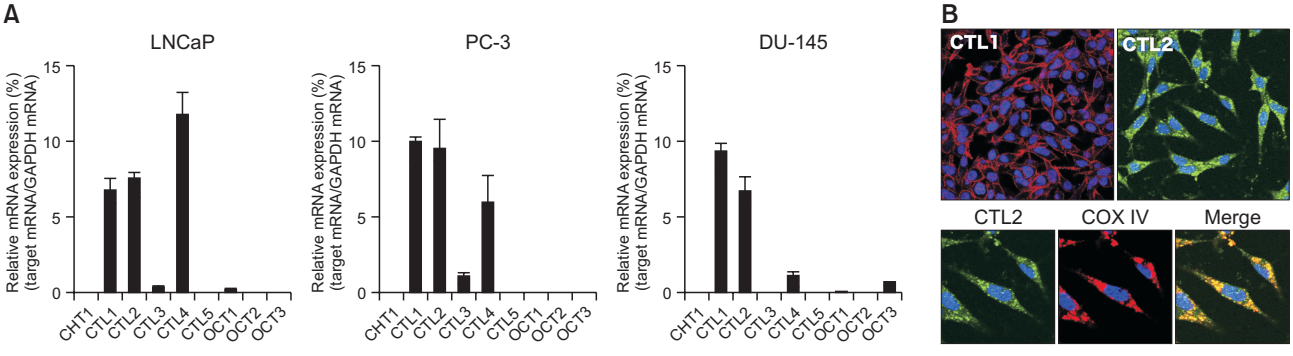

Fig. 1. Expression of choline transporters in prostate cancer cell lines, LNCaP, PC-3, and DU-145. (A) Real-time PCR analysis of CHT1, CTL1-5, and OCT1-3 expression. Relative expression is expressed as a ratio of the target mRNA to GAPDH mRNA. Experiments were performed in triplicate. Data are presented as the mean ± SD (n=3). (B) Subcellular distribution of CTL1 and CTL2 proteins by immunocytochemistry. CTL1 (red), CTL2 (green), and COX IV (red) were imaged using confocal microscopy. Nuclei were stained with DAPI (blue). Merged images are shown in Merge with yellow representing co-localization.

It has been reported that human CTL4 protein functions as thiamine pyrophosphate (TPP) transporter, and CTL4 transport TPP but not thiamine and choline (Nabokina *et al*., 2014). Therefore, CTL4 may not be involved in choline uptake in LNCaP cells. Expression of both CTL1 and CTL2 in LNCaP cells on the protein level was established by immunocytochemical staining (Fig. 1B). CTL1 was located in the plasma membrane. In contrast, CTL2 co-localized with COX IV, indicating that it was located in mitochondria.

Properties of [^{3}H]choline uptake into LNCaP cells

We examined the time course of [^{3}H]choline uptake in LNCaP cells in the presence and absence of extracellular Na^+ for 60 min (Fig. 2A). [^{3}H]Choline uptake increased in a time-dependent manner and was linear for up to 20 min. When the NaCl in the uptake buffer was replaced by NMDG-Cl, the uptake of [^{3}H]choline under Na^+-free conditions was slightly decreased compared to uptake under normal conditions.

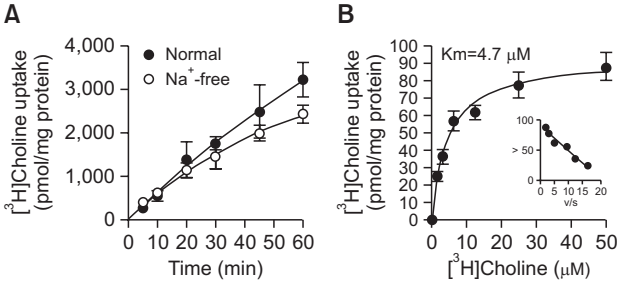

Fig. 2. Time course and Na^+-dependence of [^{3}H]choline uptake in LNCaP cells. (A) Time course of [^{3}H]choline uptake (10 μM) in the presence (●) and absence (○) of extracellular Na^+ in LNCaP cells over 60 min. Na^+-free buffer was modified by replacing NaCl with an equimolar concentration of NMDG-Cl. The time course of [^{3}H]choline uptake was fitted to the experimental data using linear regression. (B) The kinetics of [^{3}H]choline uptake in LNCaP cells. Cells were incubated for 20 min with 2.31 to 50 μM [^{3}H]choline. Inset: Eadie-Hofstee plots of [^{3}H]choline uptake show single straight lines. All data are presented as the mean ± SD (n=4).

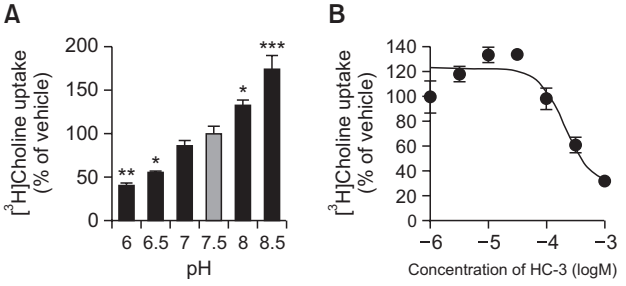

Fig. 3. Effects of pH and HC-3 treatment on [^{3}H]choline uptake in LNCaP cells. (A) Influence of extracellular pH on [^{3}H]choline uptake in LNCaP cells. [^{3}H]choline uptake (10 μM) was measured for 20 min under different pH conditions. Data are presented as a percentage of uptake relative to that at pH 7.5. *p<0.05, **p<0.01, and ***p<0.001 compared to pH 7.5. (B) Effect of HC-3 on [^{3}H]choline uptake in LNCaP cells. Cells were pre-incubated for 20 min with increasing concentrations of HC-3 followed by the measurement of [^{3}H]choline uptake for 20 min. Results are shown as a percentage of the uptake for the vehicle control. All data are presented as the mean ± SD (n=4).

The kinetics of [^{3}H]choline uptake were determined by non-linear regression. This analysis yielded a Michaelis–Menten constant (K_m) of 4.7 ± 0.7 μM and maximal velocity (V_{max}) of 93.4 ± 3.7 pmol/mg protein/min (Fig. 2B). The Eadie–Hofstee plot shows single straight lines. These data suggest that [^{3}H]choline uptake in LNCaP cells is mediated by a single Na^+-independent, intermediate-affinity transport system.

It has been reported that choline uptake through CTL1 is pH-dependent (Inazu *et al*., 2005). Therefore, the influence of extracellular pH on the uptake of [^{3}H]choline in LNCaP cells was examined by varying the pH of the pre-incubation and incubation media from pH 6.0 to 8.5 (Fig. 3A). [^{3}H]Choline uptake significantly decreased when the extracellular pH was lowered from 7.5 to 6.0. Conversely, [^{3}H]Choline uptake was enhanced when the pH of the extracellular medium was raised from 7.5 to 8.5.

HC-3 is a choline uptake inhibitor (Inazu, 2014). We investigated the inhibitory effects of this compound on the uptake of [^{3}H]choline into LNCaP cells (Fig. 3B). HC-3 inhibited [^{3}H]choline uptake in a concentration-dependent manner with a K_i of 67.3 μM.

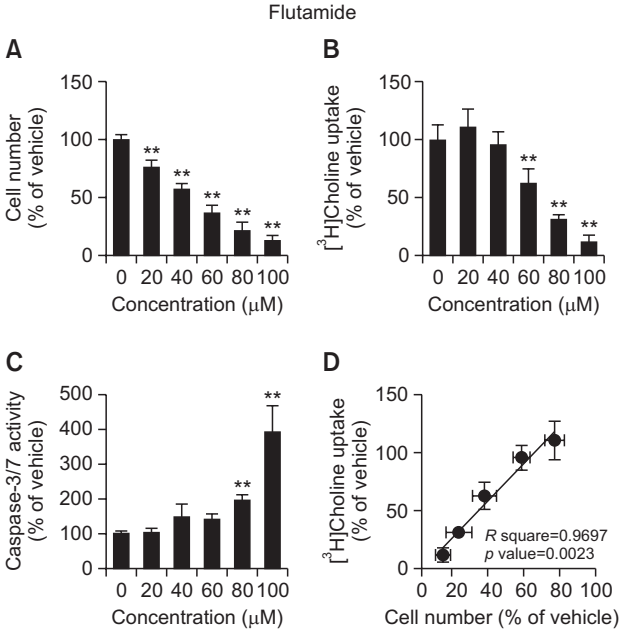

Fig. 4. Effects of flutamide on cell viability, [^{3}H]choline uptake, and caspase-3/7 activity in LNCaP cells. (A) Cell viability was measured 24 h after treatment with increasing concentrations of flutamide. The results are presented as the percentage of the vehicle control. (B) LNCaP cells were incubated for 20 min with increasing concentrations of flutamide followed by the measurement of [^{3}H]choline uptake. [^{3}H]Choline uptake was calculated as uptake per protein. The results are presented as the percentage of uptake in the vehicle control sample. (C) Cells were incubated for 24 h with increasing concentrations of flutamide followed by the measurement of caspase-3/7 activity and cell number. Caspase activity was calculated as the activity per cell number. The results are shown as a percentage of the vehicle control. (D) Correlation analysis between inhibition of [^{3}H]choline uptake and cell viability for LNCaP cells treated with increasing concentrations of flutamide. The correlation was highly statistically significant (p=0.0023) with a correlation coefficient of R square=0.9697. Data for all assays are presented as the mean ± SD (n=4). **p<0.01 compared with vehicle.

Effects of flutamide and bicalutamide on LNCaP cells

The anticancer drugs, flutamide and bicalutamide, inhibited cell viability and [^{3}H]choline uptake in a concentration-dependent manner (Fig. 4, 5). The correlations between the effects of both anticancer drugs on cell viability and [^{3}H]choline uptake were significant (flutamide *R* square=0.9697, *p*=0.0023; bicalutamide *R* square=0.9329, *p*=0.0075). Caspase-3/7 activity was significantly increased following 24 h treatment with 80 and 100 μM flutamide or 100 μM bicalutamide.

Because both flutamide and bicalutamide reduced choline uptake in LNCaP cells, we determined whether these two drugs had an effect on CTL1 protein levels in this cell line and found that both drugs (100 μM for 24 h treatment) significantly decreased the levels of this transporter (Fig. 6).

DISCUSSION

The levels of choline and phospholipid metabolites in cancer tissues have been reported to correlate with the Gleason score and tumor growth in prostate cancer patients (van Asten *et al*., 2008). Choline PET is used clinically as a diagnostic imaging technique for prostate cancer and for monitoring prostate cancer recurrence (Reske *et al*., 2006; Rinnab *et al*., 2007). However, which choline transporters are expressed in prostate cancer is currently unknown. Therefore, we analyzed the functional expression of choline transporters in the human prostate cancer cell line LNCaP. We found that CTL1, CTL2, and CTL4 were highly expressed. Human CTL4 has been shown to transport TPP but not thiamine or choline (Nabokina *et al*., 2014). Therefore, CTL4 is not likely involved in choline transport in LNCaP cells. We previously reported that CTL1 and CTL2 are highly expressed in various cancer cells types (Inazu *et al*., 2013; Taguchi *et al*., 2014; Nishiyama *et al*., 2016; Nagashima *et al*., 2018). Therefore, we examined the intracellular localization of CTL1 and CTL2 in LNCaP cells. CTL1 was clearly distributed in the plasma membrane, while CTL2 was localized to the intracellular compartment, specifically in mitochondria. These results suggest that it is CTL1 that is involved in the uptake of extracellular choline into cells, whereas CTL2 is involved in mitochondrial choline transport. These findings are similar to previous reports in which CTL1 is a target molecule for cancer therapy in esophageal cancer cells (Nagashima *et al*., 2018). We believe that CTL1 is a therapeutic target molecule not only for esophageal cancer but also for prostate cancer.

Choline oxidase is located in the inner membrane of mitochondria in the liver and kidney (Porter *et al*., 1992; Kaplan *et al*., 1993; O'Donoghue *et al*., 2009). Therefore, intracellular choline must cross the mitochondrial inner membrane before oxidation can occur. CTL2 may play an important role as the rate-limiting step of choline uptake into mitochondria. We examined whether CTL1 was involved in choline transport in LNCaP cells. LNCaP cells have a Na^+-independent and intermediate-choline transport systems. The K_m value was 4.7 μM, which is similar to those in the human cell line, and these cell types show properties similar to those of CTL1. Müller *et al*. (2009) also evaluated the sodium dependence of choline uptake in LNCaP cells. They reported that choline uptake in LNCaP cells consists of two components, 50% NaCl-dependent, and 50% NaCl-independent (Müller *et al*., 2009). However, our results showed only a Na^+-independent choline uptake mechanism. These differences may be due to the problem in

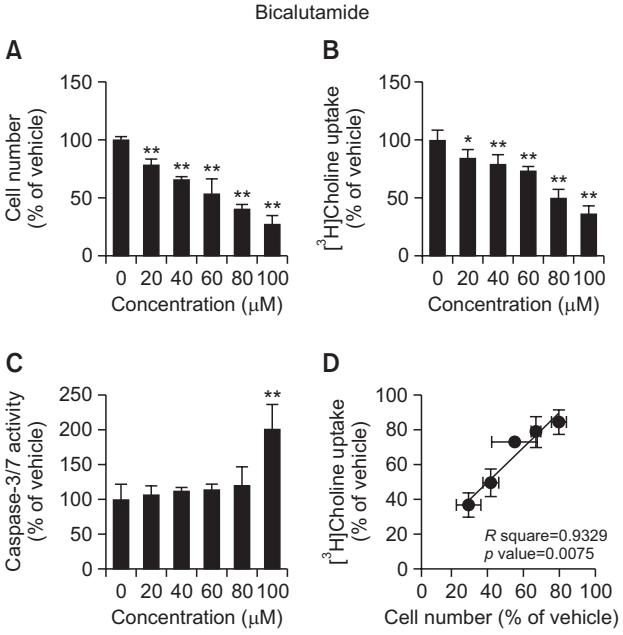

Fig. 5. Effect of bicalutamide on cell viability, [^{3}H]choline uptake, and caspase-3/7 activity in LNCaP cells. (A) Cell viability was measured 24 h after treatment with increasing concentrations of flutamide. The results are presented as the percentage of the vehicle control. (B) LNCaP cells were incubated for 20 min with increasing concentrations of bicalutamide followed by the measurement of [^{3}H]choline uptake. [^{3}H]Choline uptake was calculated as uptake per protein. The results are presented as the percentage of uptake in the vehicle control sample. (C) Cells were incubated for 24 h with increasing concentrations of bicalutamide followed by the measurement of caspase-3/7 activity and cell number. Caspase activity was calculated as the activity per cell number. The results are shown as a percentage of the vehicle control. (D) Correlation analysis between inhibition of [^{3}H]choline uptake and cell viability for LNCaP cells treated with increasing concentrations of bicalutamide. The correlation was highly statistically significant (*p*=0.0075) with a correlation coefficient of *R* square=0.9329. Data for all assays are presented as the means ± SD (n=4). ***p*<0.01 compared with vehicle.

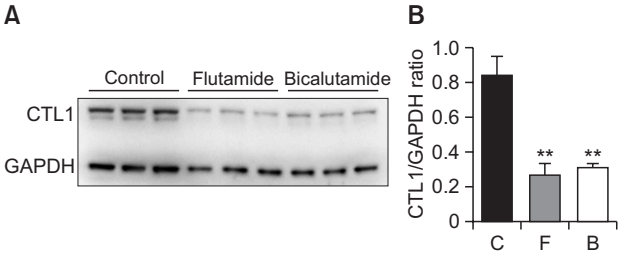

Fig. 6. Effect of flutamide and bicalutamide on CTL1 protein levels in LNCaP cells. Cells were incubated with 100 μM flutamide (F) and bicalutamide (B) for 24 h. Western blot analysis (A) and densitometry (B) show CTL1 levels in total cell lysates from drug-treated LNCaP cells. The bar graph represents the densitometric measurement of CTL1 protein normalized to GAPDH. The experiment was performed in triplicate. The densitometric data are presented as the means ± SD. ***p*<0.01 compared with control (C).

the replacement of NaCl with NMDG. In our experiment, the Cl ion concentration was maintained by replacing NaCl with NMDG chloride (NMDG-Cl). It is considered that choline uptake was inhibited by 50% as a result of replacing NaCl with NMDG alone and using a buffer solution containing 140 mM of less Cl ions. CTL1 is known to be pH-dependent and can be completely inhibited by HC-3 in the μM range (Inazu *et al*., 2013; Nishiyama *et al*., 2016; Nagashima *et al*., 2018). In this study, [^{3}H]choline uptake in LNCaP cells was decreased by acidification and increased by alkalinization of the extracellular medium, indicating that choline may be transported by a choline/H^+ antiport system in these cells. Moreover, the K_i value of HC-3 is 67.3 μM, which is very close to the K_i value for CTL1. Thus, [^{3}H]choline uptake in LNCaP cells may be mediated by CTL1.

Flutamide and bicalutamide are nonsteroidal androgen receptor antagonists that are used in the treatment of prostate cancer (Crawford *et al*., 2018). LNCaP cells are androgen-dependent prostate cancers, and these antiandrogenic drugs appear to have antiproliferative effects. Therefore, we investigated the relationship between the antitumor effects of these antiandrogens and choline uptake. Both flutamide and bicalutamide inhibited cell viability and choline uptake in LNCaP cells, and these inhibitory effects were significantly correlated. In addition, both drugs increased caspase-3/7 activity at high concentrations. Thus, both flutamide and bicalutamide were found to have not only antiandrogenic activity but also apoptosis-inducing activity by inhibiting choline uptake. Flutamide and bicalutamide are organic cationic drugs that may competitively inhibit the uptake of choline, which is an organic cation. Many studies have reported that various organic cations inhibited choline uptake and cell viability (Yamada *et al*., 2011; Nishiyama *et al*., 2016; Nagashima *et al*., 2018). These results demonstrate that the functional inhibition of choline uptake through CTL1 could promote apoptotic cell death.

After the androgen testosterone is enzymatically converted to dihydrotestosterone, it binds to the androgen receptor, which is then translocated to the nucleus, and binds to DNA, leading to the growth of prostate cancer (Choong and Wilson, 1998). Thus, the androgen receptor complex may regulate the expression of the CTL1 gene in LNCaP cells. Indeed, both flutamide and bicalutamide caused a decrease in CTL1 protein levels in LNCaP cells. Thus, the antitumor activity of flutamide and bicalutamide is thought to be involved not only in direct inhibition of CTL1-mediated choline uptake but also in suppression of CTL1 expression.

The current study suggests that LNCaP cells express the intermediate-affinity choline transporter CTL1, which uses a directed H^+ gradient as a driving force. Choline uptake through CTL1 is correlated with cell viability, and the functional inhibition of CTL1 could promote apoptotic cell death. The antiandrogens flutamide and bicalutamide may express antitumor activity through the suppression of CTL1 function and expression. Thus, the CTL1-mediated choline transport system may be a potential new target for prostate cancer therapy.

CONFLICT OF INTEREST

The authors have declared that there are no conflicts of interest.

ACKNOWLEDGMENTS

This work was supported by JSPS KAKENHI Grant Number 17K08315.

REFERENCES

Anderson, O. S., Sant, K. E. and Dolinoy, D. C. (2012) Nutrition and epigenetics: an interplay of dietary methyl donors, one-carbon metabolism, and DNA methylation. *J. Nutr. Biochem.* **23**, 853-859.

Cheng, Y. and Prusoff, W. H. (1973) Relationship between the inhibition constant (Ki) and the concentration of inhibitor which causes 50 percent inhibition (IC50) of an enzymatic reaction. *Biochem. Pharmacol.* **22**, 3099-3108.

Choong, C. S. and Wilson, E. M. (1998) Trinucleotide repeats in the human androgen receptor: a molecular basis for disease. *J. Mol. Endocrinol.* **21**, 235-257.

Crawford, E. D., Schellhammer, P. F., McLeod, D. G., Moul, J. W., Higano, C. S., Shore, N., Denis, L., Iversen, P., Eisenberger, M. A. and Labrie, F. (2018) Androgen receptor targeted treatments of prostate cancer: 35 years of progress with antiandrogens. *J. Urol.* **200**, 956-966.

Hara, T., Inagaki, K., Kosaka, N. and Morita, T. (2000) Sensitive detection of mediastinal lymph node metastasis of lung cancer with 11C-choline PET. *J. Nucl. Med.* **41**, 1507-1513.

Hara, T., Kosaka, N. and Kishi, H. (1998) PET imaging of prostate cancer using carbon-11-choline. *J. Nucl. Med.* **39**, 990-995.

Inazu, M. (2014) Choline transporter-like proteins CTLs/SLC44 family as a novel molecular target for cancer therapy. *Biopharm. Drug Dispos.* **35**, 431-449.

Inazu, M., Takeda, H. and Matsumiya, T. (2005) Molecular and functional characterization of an Na^+-independent choline transporter in rat astrocytes. *J. Neurochem.* **94**, 1427-1437.

Inazu, M., Yamada, T., Kubota, N. and Yamanaka, T. (2013) Functional expression of choline transporter-like protein 1 (CTL1) in small cell lung carcinoma cells: a target molecule for lung cancer therapy. *Pharmacol. Res.* **76**, 119-131.

Kaplan, C. P., Porter, R. K. and Brand, M. D. (1993) The choline transporter is the major site of control of choline oxidation in isolated rat liver mitochondria. *FEBS Lett.* **321**, 24-26.

Kobori, O., Kirihara, Y., Kosaka, N. and Hara, T. (1999) Positron emission tomography of esophageal carcinoma using (11)C-choline and (18)F-fluorodeoxyglucose: a novel method of preoperative lymph node staging. *Cancer* **86**, 1638-1648.

Kotzerke, J., Prang, J., Neumaier, B., Volkmer, B., Guhlmann, A., Kleinschmidt, K., Hautmann, R. and Reske, S. N. (2000) Experience with carbon-11 choline positron emission tomography in prostate carcinoma. *Eur. J. Nucl. Med.* **27**, 1415-1419.

Michel, V. and Bakovic, M. (2012) The ubiquitous choline transporter SLC44A1. *Cent. Nerv. Syst. Agents Med. Chem.* **12**, 70-81.

Michel, V., Yuan, Z., Ramsubir, S. and Bakovic, M. (2006) Choline transport for phospholipid synthesis. *Exp. Biol. Med. (Maywood)* **231**, 490-504.

Müller, S. A., Holzapfel, K., Seidl, C., Treiber, U., Krause, B. J. and Senekowitsch-Schmidtke, R. (2009) Characterization of choline uptake in prostate cancer cells following bicalutamide and docetaxel treatment. *Eur. J. Nucl. Med. Mol. Imaging* **36**, 1434-1442.

Nabokina, S. M., Inoue, K., Subramanian, V. S., Valle, J. E., Yuasa, H. and Said, H. M. (2014) Molecular identification and functional characterization of the human colonic thiamine pyrophosphate transporter. *J. Biol. Chem.* **289**, 4405-4416.

Nagashima, F., Nishiyama, R., Iwao, B., Kawai, Y., Ishii, C., Yamanaka, T., Uchino, H. and Inazu, M. (2018) Molecular and functional characterization of choline transporter-like proteins in esophageal cancer cells and potential therapeutic targets. *Biomol. Ther. (Seoul)* **26**, 399-408.

Nishiyama, R., Nagashima, F., Iwao, B., Kawai, Y., Inoue, K., Midori, A., Yamanaka, T., Uchino, H. and Inazu, M. (2016) Identification and functional analysis of choline transporter in tongue cancer: a novel molecular target for tongue cancer therapy. *J. Pharmacol.*

Sci. **131**, 101-109.

O'Donoghue, N., Sweeney, T., Donagh, R., Clarke, K. J. and Porter, R. K. (2009) Control of choline oxidation in rat kidney mitochondria. *Biochim. Biophys. Acta* **1787**, 1135-1139.

Ohtani, T., Kurihara, H., Ishiuchi, S., Saito, N., Oriuchi, N., Inoue, T. and Sasaki, T. (2001) Brain tumour imaging with carbon-11 choline: comparison with FDG PET and gadolinium-enhanced MR imaging. *Eur. J. Nucl. Med.* **28**, 1664-1670.

Porter, R. K., Scott, J. M. and Brand, M. D. (1992) Choline transport into rat liver mitochondria. Characterization and kinetics of a specific transporter. *J. Biol. Chem.* **267**, 14637-14646.

Reske, S. N., Blumstein, N. M., Neumaier, B., Gottfried, H. W., Finsterbusch, F., Kocot, D., Möller, P., Glatting, G. and Perner, S. (2006) Imaging prostate cancer with 11C-choline PET/CT. *J. Nucl. Med.* **47**, 1249-1254.

Rinnab, L., Blumstein, N. M., Mottaghy, F. M., Hautmann, R. E., Küfer, R., Hohl, K. and Reske, S. N. (2007) 11C-choline positron-emission tomography/computed tomography and transrectal ultrasonography for staging localized prostate cancer. *BJU Int.* **99**, 1421-1426.

Schwarzenböck, S., Souvatzoglou, M. and Krause, B. J. (2012) Choline PET and PET/CT in primary diagnosis and staging of prostate cancer. *Theranostics* **2**, 318-330.

Taguchi, C., Inazu, M., Saiki, I., Yara, M., Hara, N., Yamanaka, T. and Uchino, H. (2014) Functional analysis of [methyl-(3)H]choline uptake in glioblastoma cells: influence of anti-cancer and central nervous system drugs. *Biochem. Pharmacol.* **88**, 303-312.

Tian, M., Zhang, H., Oriuchi, N., Higuchi, T. and Endo, K. (2004) Comparison of 11C-choline PET and FDG PET for the differential diagnosis of malignant tumors. *Eur. J. Nucl. Med. Mol. Imaging* **31**, 1064-1072.

van Asten, J. J, Cuijpers, V., Hulsbergen-van de Kaa, C., Soede-Huijbregts, C., Witjes, J. A., Verhofstad, A. and Heerschap, A. (2008) High resolution magic angle spinning NMR spectroscopy for metabolic assessment of cancer presence and Gleason score in human prostate needle biopsies. *MAGMA* **21**, 435-442.

Xu, K. M., Chen, R. C., Schuster, D. M. and Jani, A. B. (2019) Role of novel imaging in the management of prostate cancer. *Urol. Oncol.* **37**, 611-618.

Yamada, T., Inazu, M., Tajima, H. and Matsumiya, T. (2011) Functional expression of choline transporter-like protein 1 (CTL1) in human neuroblastoma cells and its link to acetylcholine synthesis. *Neurochem. Int.* **58**, 354-365.